Editors' Suggestion

Chemical migration and dipole formation at van der Waals interfaces between magnetic transition metal chalcogenides and topological insulators

Brenton A. Noesges,[1,*] Tiancong Zhu,[1] Jacob J. Repicky,[1] Sisheng Yu,[1] Fengyuan Yang,[1] Jay A. Gupta,[1] Roland K. Kawakami,[1] and Leonard J. Brillson[1,2]

[1]*Department of Physics, The Ohio State University, Columbus, Ohio 43210, USA*

[2]*Department of Electrical and Computer Engineering, The Ohio State University, Columbus, Ohio 43210, USA*

(Received 21 February 2020; accepted 13 April 2020; published 8 May 2020)

This paper is a contribution to the joint Physical Review Applied *and* Physical Review Materials *collection titled Two-Dimensional Materials and Devices.*

Metal and magnetic overlayers alter the surface of the topological insulator (TI) bismuth selenide (Bi_2Se_3) through proximity effects but also by changing the composition and chemical structure of the Bi_2Se_3 subsurface. The interface between Bi_2Se_3 and Mn metal or manganese selenide was explored using x-ray photoelectron spectroscopy revealing chemical and electronic changes at the interface. Depositing Mn metal on Bi_2Se_3 without an external source of Se shows unexpected bonding within the Mn layer due to Mn-Se bonding as Se diffuses out of the Bi_2Se_3 layer into the growing Mn film. The Se outdiffusion is further evidenced by changes in Bi core levels within the Bi_2Se_3 layers indicating primarily Bi-Bi bonding over Bi-Se bonding. No outdiffusion of Se occurred when excess Se is supplied with Mn, indicating the importance of supplying enough chalcogen atoms with deposited metals. However, Bi_2Se_3 core-level photoelectrons exhibited a rigid chemical shift toward higher binding energy after depositing a monolayer of $MnSe_{2-x}$, indicating a dipole within the overlayer. Stoichiometry calculations indicated that the monolayer forms MnSe preferentially over the transition metal dichalcogenide (TMD) phase $MnSe_2$, providing a consistent picture of the dipole formation in which a plane of Se anions sits above Mn cations. This study shows that chemical diffusion and dipole formation are important for Mn-Bi_2Se_3 and $MnSe_{2-x}Bi_2Se_3$ and should be considered carefully for TMD/TI interfaces more generally.

DOI: 10.1103/PhysRevMaterials.4.054001

I. INTRODUCTION

Proximity effects between materials can induce new properties at their interface that would not otherwise exist separately. Magnetic overlayers brought into contact with topological insulators (TIs) such as Bi_2Se_3 can break time-reversal symmetry and affect spin properties leading to quantum phenomena, i.e., the quantum anomalous Hall effect (QAHE) [1,2] and skyrmions [3]. Three-dimensional (3D) ferromagnets such as α-MnSe (111) or even two-dimensional (2D) materials such as 1*T*-$MnSe_2$ [4] are promising candidates to induce these surface magnetic and spin-related effects in Bi_2Se_3 [5]. A crucial component to realizing these advanced interface effects is an abrupt and clean interface between Bi_2Se_3 and the ferromagnetic overlayer, particularly for $MnSe_2$, which is a van der Waals (vdW) material with only weak bonding between layers. Molecular beam epitaxy (MBE) growth and subsequent transfers to measurement systems carried out completely in ultrahigh vacuum (UHV) provided a method to create and analyze high-quality interfaces without interlayer contamination or surface oxidation. Interlayer contaminants can alter the interface electronic and magnetic properties, and the electronic properties of both constituents will begin to degrade if exposed to oxygen. While UHV helps remove external contaminants, interdiffusion and other chemical interaction at the interface between Bi_2Se_3 and the magnetic overlayer can still occur. Many metals including Mn have been used to dope or alloy with Bi_2Se_3 [6] so that the chemical interaction between the two layers could in principle dominate the electronic and magnetic properties at their interface [7,8]. Furthermore, Mn and Bi_2Se_3 can form a magnetic ternary alloy Bi_2MnSe_4, which is also a promising system to investigate novel quantum and topological states [9–11].

Surface-sensitive techniques such as x-ray photoelectron spectroscopy (XPS) can provide insight into the impact of Mn-containing overlayers on the electronic structure of Bi_2Se_3 and how Mn incorporates with Bi_2Se_3 at the $MnSe_2$ interface. We used XPS connected via a UHV suitcase to a MBE system to investigate chemical interaction at the interface between a selenide transition metal dichalcogenide (TMD) and Bi_2Se_3. We compared the chemical effects on pristine Bi_2Se_3 of Mn-containing overlayers in two different scenarios: (i) extreme Se-deficient case, i.e., Mn deposited alone onto Bi_2Se_3, and (ii) Mn deposited with excess Se. In the case of pure Mn metal on Bi_2Se_3 we saw that Mn reacts with the Bi_2Se_3 surface where Mn bonds with Se extracted by diffusion from the Bi_2Se_3 substrate. In contrast, when excess Se was provided, there was little chemical interaction observed at the interface between $MnSe_{2-x}$ and Bi_2Se_3. Instead, $MnSe_{2-x}$ on Bi_2Se_3 rigidly shifted subsurface Bi_2Se_3 core levels toward higher binding energy, indicating the

*noesges.1@osu.edu

formation of a negative surface/interface dipole. The presence of this dipole is likely due to the growth of primarily α-MnSe instead of the $1T$-$MnSe_2$ 2D phase, which is supported by topographic scanning tunneling microscopy (STM) images and spectroscopy. Our XPS core level analysis combined with controlled depositions, air-free transfers, and surface analysis provides a consistent picture of chemical diffusion and dipole formation at the Mn selenide/Bi_2Se_3 junction, revealing interfacial effects that may be relevant to TMD/TI heterostructures in general.

II. METHODS

A. Molecular beam epitaxy

Prior to Bi_2Se_3 sample growth, $Al_2O_3(0001)$ substrates were annealed in the air at 1000 °C for 3 h. The substrates were then transferred to a home-built molecular beam epitaxy (MBE) chamber and heated to a growth temperature of 250 °C. Bi and Se were evaporated from standard Knudsen cells. A Se/Bi flux ratio (by thickness) of 20:1 was used during the growth with the Bi cell at 575 °C and the Se cell at 180 °C. Bi_2Se_3 was deposited at a growth rate of 1 nm/min. After the growth, the samples were cooled down to room temperature in vacuum. A 20 nm Se capping layer was deposited on top of Bi_2Se_3 to prevent oxidation before taking the sample out of the chamber.

Both Mn-Bi_2Se_3 and $MnSe_{2-x}$-Bi_2Se_3 were grown in a separate MBE chamber (Veeco GEN930). The Se-capped Bi_2Se_3 samples were mounted onto 18 mm flag style paddles and loaded into the MBE chamber using special adapters to the 75 mm uniblock sample plates. The samples were first gently annealed at 170 °C to remove the Se capping. Reflection high-energy electron diffraction (RHEED) was used to monitor the sample surface and ensure that the cap removal is complete. During deposition, both Mn and Se were evaporated from a Knudsen cell. For the Mn-Bi_2Se_3 sample, Mn was deposited at room temperature with a beam flux of 5×10^{-9} torr. For the $MnSe_{2-x}$-Bi_2Se_3 sample, Mn and Se were codeposited at 250 °C with a flux ratio of $\sim 1:50$ (by beam equivalent pressure).

B. *In vacuo* transfer and XPS measurement

To prevent oxidation, all samples were transferred between the $MnSe_{2-x}$ growth chamber and XPS chamber using an ultrahigh vacuum (UHV) suitcase tool that carries the 18 mm sample paddles. XPS measurements provided chemical composition and bonding information for the decapped Bi_2Se_3 surface and two overlayer samples, 1.5 nm of Mn metal and 1 monolayer (ML) of $MnSe_{2-x}$.

XPS was performed using a PHI VersaProbe 5000^{TM} system equipped with a Scanning XPS Microprobe X-ray source ($h\upsilon_{AlK\alpha} = 1486.6$ eV; full width at half-maximum $\leqslant 0.5$ eV), and a hemispherical energy analyzer with a pass energy of 23.5 eV and a 0.05 eV step. To minimize the effects of charging, the XPS system is equipped with a two-stage sample surface neutralization system consisting of a 10 eV electron flood gun accompanied by a 10 eV Ar^+ ion beam. Photoelectrons were collected at a takeoff angle of 45°. Chemical composition was determined using the PHI MultiPak analysis suite to determine relative atomic concentration using relative sensitive factors [12] for Bi $5d$, Bi $4f$, Se $3d$, and Mn $2p$ core levels of 26.089, 180.178, 14.492, and 53.366, respectively. Additional curve fitting was performed using asymmetric Gaussian or Voigt line shapes for metallic and nonmetallic states, respectively.

TABLE I. Stoichiometry found by determining relative peak areas below Se $3d$, Mn $2p$, and an average of the Bi $4f$ and Bi $5d$ core levels. Peak areas were normalized with relative sensitivity factors appropriate for each core level. The Mn:Se ratio was estimated for the case of $MnSe_{2-x}$ on Bi_2Se_3 by assuming the Bi:Se ratio as found in the bare Bi_2Se_3 surface.

	Bi_2Se_3	Mn/Bi_2Se_3	$MnSe_{2-x}/Bi_2Se_3$
% Bi	50.9 ± 0.7	45.0 ± 1.0	40.9 ± 0.6
% Se	49.1 ± 0.8	31.0 ± 1.0	49.2 ± 0.7
% Mn		24.5 ± 0.6	9.9 ± 0.5
Bi:Se ratio	1.03 ± 0.02	1.47 ± 0.06	Assuming 1.03
Mn:excess Se ratio			1.0 ± 0.1

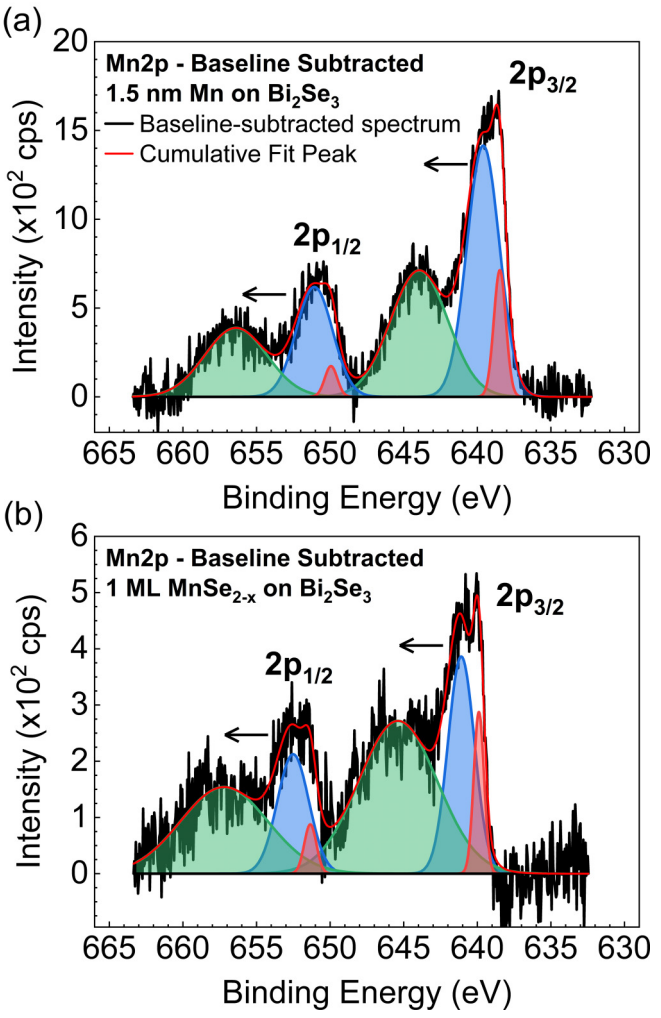

FIG. 1. Mn $2p$ core level spectrum of deposited Mn metal indicating unexpected Mn-Se bonding as shown by satellite features in green shifted to higher binding energy as indicated by the arrows. (b) $MnSe_{2-x}$ Mn $2p$ core level showing similar satellite features indicating Mn-Se bonding.

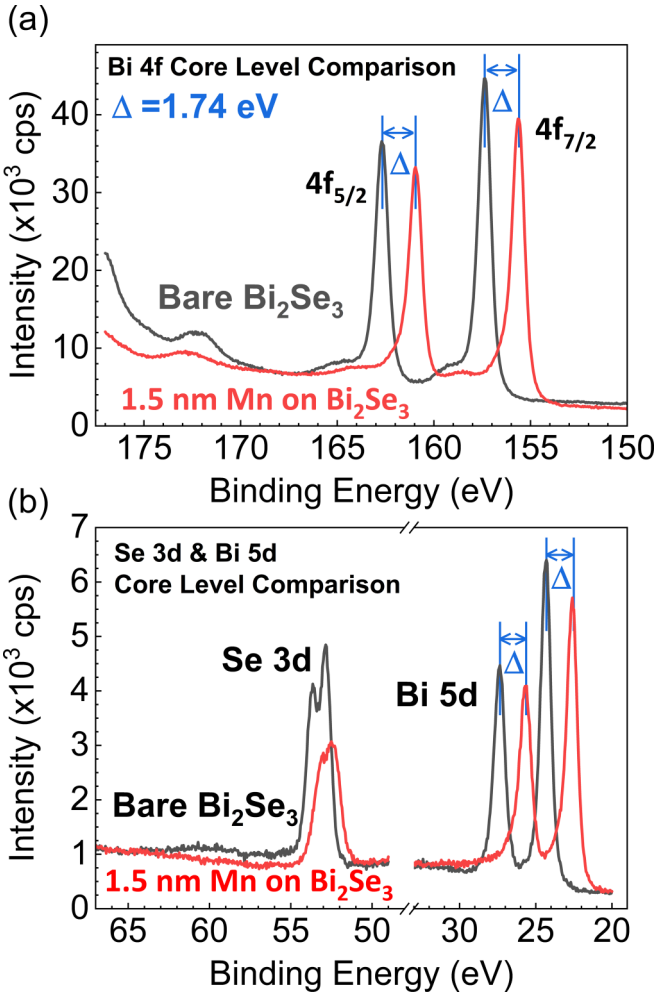

FIG. 2. (a) Bi 4f core level showing the binding energy difference before (black) and after (red) 1.5 nm Mn deposition. Depositing 1.5 nm of Mn causes Bi core levels of Bi_2Se_3 to shift toward higher binding energy. (b) Se 3d and Bi 5d core levels. The Se 3d peaks do not exhibit the same 1.74 eV shift as the Bi core levels.

C. STM measurement

STM measurements were performed at 5 K using a CreaTec LT-STM. Samples were transferred from the MBE growth chamber to the STM system through a UHV suitcase to preserve the as-grown quality of the films. No additional preparation of the surface was performed prior to measurement. Images were obtained in constant current mode with a setpoint of 50–500 pA and sample bias in the range of 0.5–1 V. Tunneling spectra were obtained by adding a 20–50 mV modulation voltage at 1063 Hz to the dc bias and measured using a lock-in amplifier. Image processing and analysis were performed using WxSM [13].

III. RESULTS

A. Bare Bi_2Se_3 surface

The bare surface of decapped Bi_2Se_3 was first studied to check for surface contamination and establish a baseline for Bi and Se XPS peak centers and stoichiometry. Wide energy range XPS surveys and detailed region scans showed

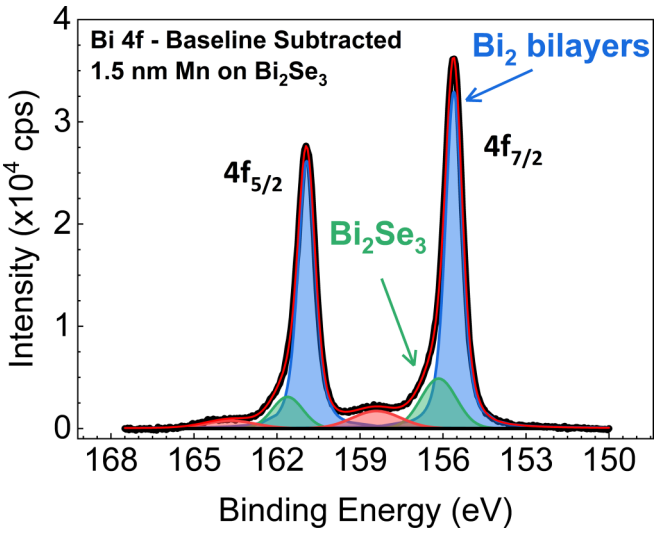

FIG. 3. Deconvolved Bi 4f core level spectra for 1.5 nm of Mn metal on Bi_2Se_3. The dominant peak at lower binding energy is related to the formation of Bi_2 layers within Bi_2Se_3.

no detectable core level signals other than the expected Bi and Se levels and related Auger electron features. The decapped surface showed sharp Bi 5d, Bi 4f, and Se 3d doublets with binding energies (BE) consistent with previously measured Bi_2Se_3 core levels [14,15]. The stoichiometry of the Bi_2Se_3 surface (Table I) was obtained by comparing the relative peak areas below the Bi 5d, Bi 4f, and Se 3d spectra where the corrected peak areas for Bi 5d and 4f were averaged together. The Bi:Se ratio was found to be 1.03 ± 0.02 indicating a Se-deficient surface (Table I). The XPS spectra also show a pair of small broad features near the 285 eV region where a C 1s line would be. However, neither feature is a C 1s feature but instead they are related to Se Auger electron transitions [16]. Since the O 1s line was below the detection threshold of the survey scan, a detailed region scan was not performed. The lack of surface contamination of the samples transferred via a UHV suitcase confirms the quality of the suitcase transfer and its ability to maintain a clean, oxide-free sample surface.

B. Mn-Bi_2Se_3

To study the interaction of Mn metal with the Bi_2Se_3 surface, we deposited Mn metal only, e.g., without Se, onto Bi_2Se_3. The wide range survey scan [Fig. S1(a) of the Supplemental Material] shows virtually identical peaks to the bare Bi_2Se_3 surface with the addition of Mn-related peaks, notably the Mn 2p core level. Detailed region scans of the Mn 2p core level [Fig. 1(a)] show additional satellite features shifted to higher BE relative to the metallic Mn peak features. The shift to higher BE indicates Mn-Se bonding as evidenced by the increase in BE and charge state of the Mn ions. Additionally, the Mn 2p line shape is consistent with past measurement and modeling of manganese octahedrally coordinated to form MnX_6 clusters [17,18].

There are two likely sources for the Se observed in the Mn metal overlayer: (i) Se pulled from the Bi_2Se_3 layers below, or (ii) residual Se from the growth chamber. The Bi core levels provide insight into the source of this Se in the Mn

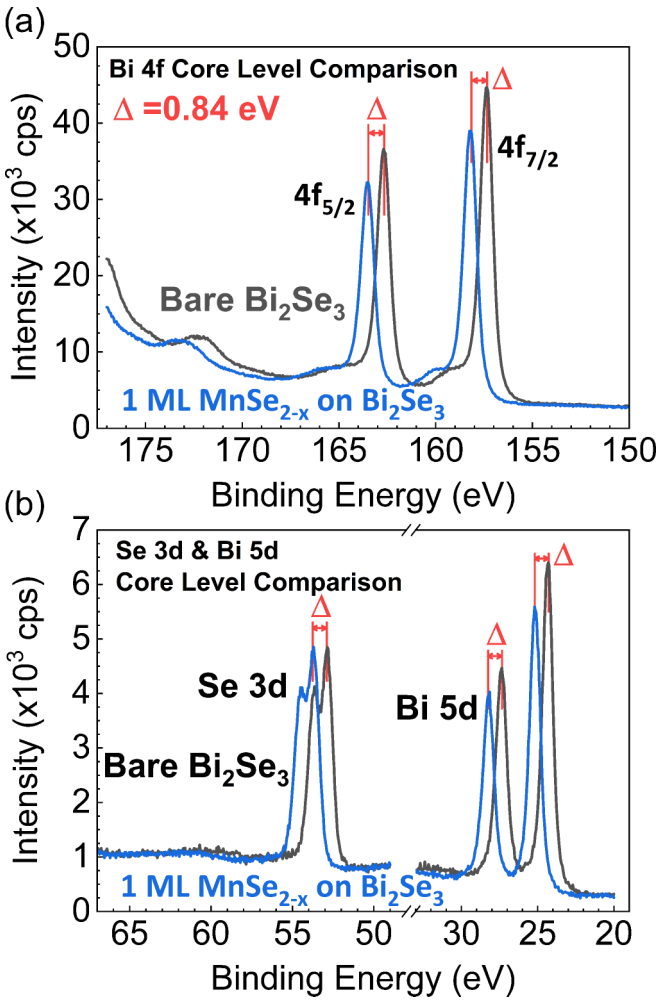

FIG. 4. (a) Bi 4f core level showing the binding energy difference before (black) and after (blue) 1 ML $MnSe_{2-x}$ deposition. (b) Se 3d and Bi 5d core levels. The Se 3d peaks do not exhibit the same 1.74 eV shift as the Bi core levels. Depositing 1 ML of $MnSe_{2-x}$ causes the Bi and Se core levels to rigidly shift 0.84 eV toward higher binding energy.

layer. Both Bi 5d and 4f core levels [Figs. 2(a) and 2(b)] exhibit a 1.74 eV shift toward lower BE after Mn metal was deposited. However, such a large negative BE shift is not seen in the Se 3d core level [Fig. 2(b)]. This large negative BE shift in bismuth core levels has been previously identified as Bi_2 layer formation within the bismuth selenide [14,19]. A careful deconvolution of the Bi 4f core level spectra (Fig. 3) reveals a small feature at higher BE compared to the dominant Bi $4f_{7/2}$ peak. This smaller feature has BE consistent with the Bi_2Se_3 previously observed, indicating that Mn is not fully converting the subsurface Bi_2Se_3 into bismuth bilayers. Such changes in the bismuth core levels were not observed in earlier XPS studies on Mn-doped Bi_2Se_3 [20]. This is evidence that the Se in the Mn layer has diffused out of the Bi_2Se_3 leaving behind Bi_2 bilayers rather than Se pulled from the surrounding chamber.

C. $MnSe_{2-x}$-Bi_2Se_3

There is a very different interface picture on the side of Bi_2Se_3 when Mn is deposited with excess Se in a growth

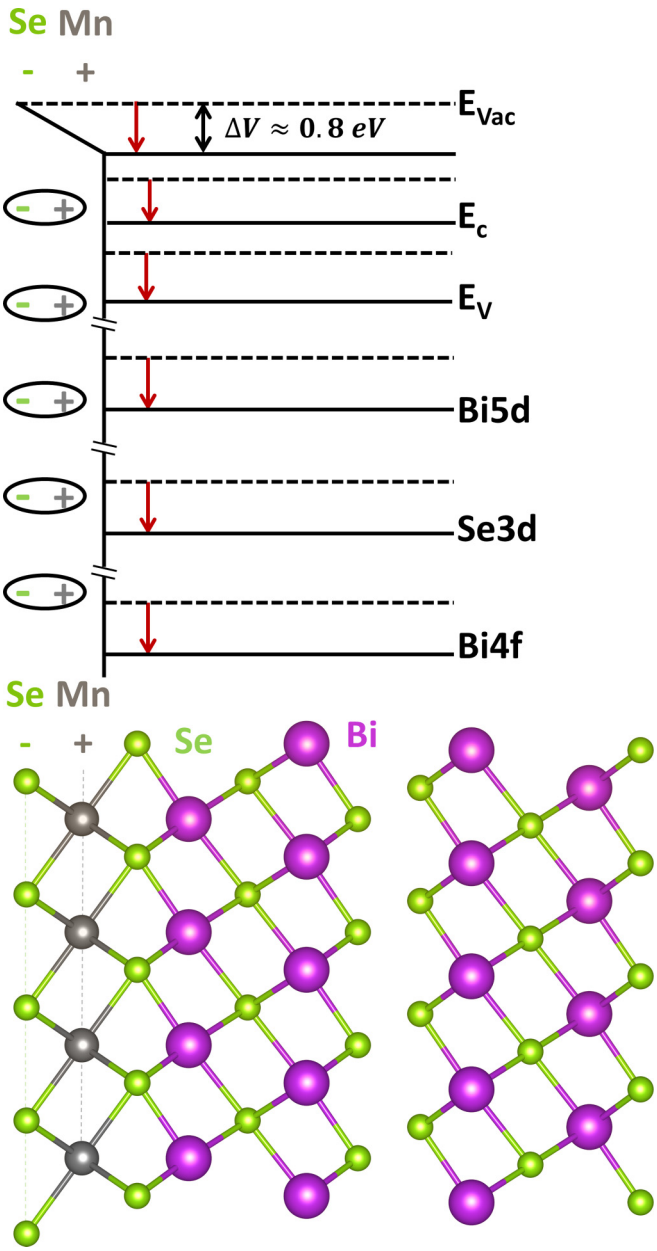

FIG. 5. Schematic band and lattice diagram showing the location of the expected dipole and the effect on the Bi_2Se_3 core levels below the TMD/TI interface. Crystal structure produced using VESTA [21].

targeted for one unit-layer of $MnSe_2$. Figure 1(b) shows that the Mn 2p core level of $MnSe_{2-x}$ shows a similar peak structure but shifted 1.4 eV toward higher BE compared to that of the deposited Mn metal on Bi_2Se_3 in Fig. 1(a). The similar deconvolved peak structure confirms that the Mn metal BE shown above is consistent with Mn-Se bonding. However, all the photoelectron BE measured from Bi_2Se_3 after depositing 1 ML $MnSe_{2-x}$ exhibit a rigid 0.8 eV chemical shift toward higher BE compared to bare Bi_2Se_3 [Figs. 4(a) and 4(b)]. This shift toward higher observed BE indicates the presence of a negative interface dipole. Given the increase in BE, such a dipole represents an extra potential barrier at the free surface that escaping core level photoelectrons most overcome, shown schematically in Fig. 5.

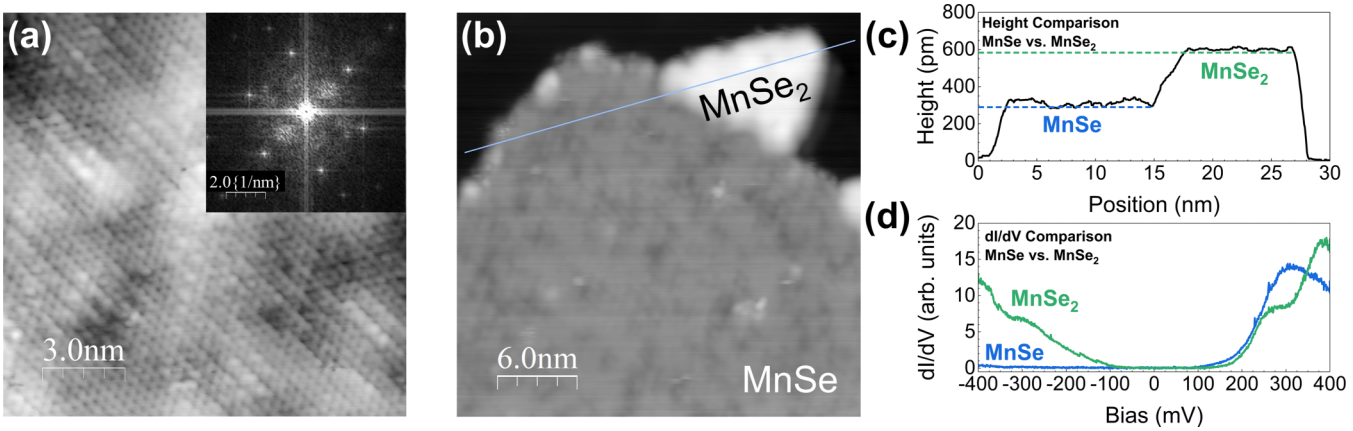

FIG. 6. (a) Atomically resolved STM image of an α-MnSe(111) island on Bi_2Se_3 (10 mV, 500 pA). The inset shows a Fourier transform image of the area with a lattice constant of 3.97 ± 0.04 Å. (b) Topographic image of a $1T$-$MnSe_2$ island adjacent to an α-MnSe(111) island (1 V, 50 pA). (c) Line profile of the two islands measured along the blue line in (b). The dashed line represents the average height of the step for MnSe (blue) and $MnSe_2$ (green). (d) Comparison of dI/dV spectroscopy collected on α-MnSe(111) (blue) and $1T$-$MnSe_2$ (green).

We used the relative peak areas below deconvolved Mn $2p$, Se $3d$, and averaged Bi $4f$ and $5d$ core level features to calculate the surface stoichiometries shown in Table I. Based on the Bi:Se ratio of 1.03 as observed for the bare Bi_2Se_3, the ratio of Mn:Se is 1.0 ± 0.1, indicating a Se deficiency, and the chemical phase of the manganese selenide overlayer is more likely MnSe instead of $MnSe_2$. The formation of MnSe versus the van der Waals material $MnSe_2$ helps explain the origin of the observed dipole. A single monolayer of MnSe would form a negatively charged plane of Se ions on positively charged Mn creating the dipole that retards exiting electrons and causes the core level shift to higher BE.

Consistent with these XPS results, STM surface characterization suggests that α-MnSe(111) is the dominant phase within the $MnSe_{2-x}$ interfacial region. Atomic resolution of a typical α-MnSe(111) island is shown in Fig. 6(a). The inset shows a Fourier transform of the area confirming well-ordered structures with triangular symmetry and a lattice constant of 3.97 ± 0.04 Å consistent with α-MnSe(111) [22]. The topographic line profiles and dI/dV spectroscopy [Figs. 6(c) and 6(d)] indicate that α-MnSe(111) islands have an apparent height of 2.9 ± 0.2 Å and an energy gap of 700 meV. The observed gap is smaller than the 3 eV gap expected for bulk α-MnSe [22], but the measured step height and atomic lattice constant is in good agreement with other measurements of α-MnSe(111) [8], consistent with our expected XPS stoichiometry. Figure 6(b) also shows that a small secondary phase distinct from α-MnSe(111) exists on the surface. In comparison to α-MnSe, these small (<10 nm diam) islands show apparent heights of 5.8 ± 0.1 Å and exhibit a distinct dI/dV spectrum [Fig. 6(d)] with a much smaller gap. This is suggestive of $1T$-$MnSe_2$ formation, but these smaller secondary phase regions are too small and low density to measure with XPS for further characterization.

IV. ANALYSIS

A. Mn-Bi_2Se_3

Pure Mn metal interacts strongly at the interface with Bi_2Se_3 where Se diffuses out of Bi_2Se_3 into the Mn overlayer creating clusters of $MnSe_{2-x}$ as indicated by the satellite features in the Mn $2p$ core level [Fig. 1(a)]. The removal of Se from Bi_2Se_3 also leaves behind metallic Bi bilayers below the interface as evidenced by the strong 1.74 eV negative binding energy shifts of the Bi $5d$ and $4f$ core levels. This Se outdiffusion has been observed in other Bi_2Se_3-metal interfaces with Cr and Fe overlayers [15]. The difference in chemical reactivity between MnSe and $MnSe_2$ may also factor into the MnSe formation. The chemical equations for Mn reaction at the surface of Bi_2Se_3 are $Mn+(1/3)Bi_2Se_3 \rightarrow MnSe+(2/3)Bi$ for MnSe, and $Mn+(2/3)Bi_2Se_3 \rightarrow MnSe_2+(4/3)Bi$ for $MnSe_2$. The heat of reaction ΔH_R per metal atom for MnSe ($H_F = -155.6$ kJ/mol) [23] versus Bi_2Se_3 ($H_F = -140.2$ kJ/mol) [24] is -108.8 kJ/mol or -1.12 eV/metal atom compared with $MnSe_2$($H_F = -180.5$ kJ/mol) versus Bi_2Se_3, which yields -87 kJ/mol or -0.90 eV/metal atom, which is less reactive.

B. $MnSe_{2-x}$-Bi_2Se_3

There is less chemical reactivity at the interface when Se is supplied alongside Mn during deposition. There is no evidence of Se outdiffusion or metallic bismuth formation below the $MnSe_{2-x}/Bi_2Se_3$ interface as there was in the case of Mn metal. However, the existence of a single monolayer of $MnSe_{2-x}$ produces a 0.74 eV rigid shift toward higher binding energy observed in Bi_2Se_3 core level photoelectrons. This increase in binding energy is due to an interface dipole created by the dominant manganese monoselenide phase that formed over the $MnSe_2$ phase. α-MnSe (111) forms a plane of negatively charged Se ions at the free surface sitting above positive Mn ions, which creates the observed negative dipole that slows escaping core level photoelectrons. Smaller regions of $MnSe_2$ also exist on the Bi_2Se_3 surface, but these regions are too small and low density to compare results between MnSe and $MnSe_2$ regions. Presumably, such a dipole would not exist in a predominantly $MnSe_2/Bi_2Se_3$ interface.

V. OUTLOOK

VdW heterostructures of 2D magnets on topological insulators hold promise for many spintronic studies including spin-orbit torque [25,26], skyrmion magnetic textures [27,28], the proximity-induced quantum anomalous Hall effect [29–31], and intrinsic magnetic topological insulators [32–34]. Our results highlight the importance of chemical analysis and atomic-scale structural characterization to help realize the desired heterostructures with abrupt interfaces and minimal chemical migration. The coexistence of tall islands (2D magnet $MnSe_2$ on topological insulator Bi_2Se_3) and short islands (MnSe covalently bonded to Bi_2Se_3 to form a septuple vdW layer) indicates a path to make either distinct 2D magnet/topological insulator heterostructures or intrinsic $MnBi_2Se_4$ by appropriate optimization of the growth conditions [35]. More generally, this provides a method for synthesizing and characterizing high-quality TMD/TI vdW heterostructures with a variety of functionalities for the TMD (e.g., semiconductor, valleytronic, superconductor, etc.).

VI. CONCLUSIONS

We have used surface-science techniques to explore the interface chemistry between Bi_2Se_3 and Mn-containing overlayers, and we found surface reactions and diffusion between constituents that depend significantly on the Se conditions during deposition. Mn metal deposited without excess Se induces Se outdiffusion from the Bi_2Se_3 substrate. This behavior suggests that Mn should be supplied with excess selenium to avoid altering the Bi_2Se_3 on which the Mn is deposited. When Se is supplied with Mn, no outdiffusion of Se occurs. Rather, Bi_2Se_3 core level photoelectrons exhibit a rigid shift toward higher binding energy, indicating a surface dipole caused by the formation of primarily α-MnSe (111) with smaller regions of $MnSe_2$. The existence of this dipole can be useful to indicate the phase of the grown manganese selenide overlayer when exact stoichiometry analysis is challenging or impossible due to a shared core level. Further, this work points to the importance of supplying excess chalcogen during deposition to avoid chemical bonding with substrate chalcogen atoms. This evidence for chemical diffusion and dipole formation at the Mn selenide/Bi_2Se_3 junction reveals interfacial effects that may be relevant to TMD/TI heterostructures in general.

ACKNOWLEDGMENTS

This research was primarily supported by the Center for Emergent Materials: an NSF MRSEC under Award No. DMR-1420451 (XPS measurements by BAN and LJB). T.Z., J.J.R., J.A.R., and R.K.K. acknowledge support from the U.S. Department of Energy (DOE), Office of Science, Basic Energy Sciences under Grant No. DE-SC0016379 (growth of Mn and Mn-selenide films and STM measurements). S.Y. and F.Y. acknowledge support from the U.S. DOE, Office of Science, Basic Energy Sciences, under Grant No. DE-SC0001304 (growth of Bi_2Se_3 films).

[1] Y. Hou, J. Kim, and R. Wu, Magnetizing topological surface states of Bi_2Se_3 with a CrI_3 monolayer, Sci. Adv. **5**, eaaw1874 (2019).

[2] S. Zhu, D. Meng, G. Liang, G. Shi, P. Zhao, P. Cheng, Y. Li, X. Zhai, Y. Lu, L. Chen, and K. Wu, Proximity-induced magnetism and an anomalous Hall effect in $Bi_2Se_3/LaCoO_3$: A topological insulator/ferromagnetic insulator thin film heterostructure, Nanoscale **10**, 10041 (2018).

[3] J. Chen, L. Wang, M. Zhang, L. Zhou, R. Zhang, L. Jin, X. Wang, H. Qin, Y. Qiu, J. Mei, F. Ye, B. Xi, H. He, B. Li, and G. Wang, Evidence for magnetic skyrmions at the interface of ferromagnet/topological-insulator heterostructures, Nano Lett. **19**, 6144 (2019).

[4] K. S. Burch, D. Mandrus, and J. Park, Magnetism in two-dimensional van der Waals materials, Nature (London) **563**, 47 (2018).

[5] W. Luo and X. L. Qi, Massive Dirac surface states in topological insulator/magnetic insulator heterostructures, Phys. Rev. B **87**, 085431 (2013).

[6] S. Y. Xu, M. Neupane, C. Liu, D. Zhang, A. Richardella, L. A. Wray, N. Alidoust, M. Leandersson, T. Balasubramanian, J. Sánchez-Barriga, O. Rader, G. Landolt, B. Slomski, J. H. Dil, J. Osterwalder, T. R. Chang, H. T. Jeng, H. Lin, A. Bansil, N. Samarth and M. Z. Hasan, Hedgehog spin texture and Berry's phase tuning in a magnetic topological insulator, Nat. Phys. **8**, 616 (2012).

[7] Y. Okuyama, R. Ishikawa, S. Kuroda, and T. Hirahara, Role of hybridization and magnetic effects in massive Dirac cones: Magnetic topological heterostructures with controlled film thickness, Appl. Phys. Lett. **114**, 051602 (2019).

[8] A. V. Matetskiy, I. A. Kibirev, T. Hirahara, S. Hasegawa, A. V. Zotov, and A. A. Saranin, Direct observation of a gap opening in topological interface states of $MnSe/Bi_2Se_3$ heterostructure, Appl. Phys. Lett. **107**, 091604 (2015).

[9] J. A. Hagmann, X. Li, S. Chowdhury, S. N. Dong, S. Rouvimov, S. Pookpanratana, K. M. Yu, T. A. Orlova, T. B. Bolin, and C. U. Segre, Molecular beam epitaxy growth and structure of self-assembled Bi_2Se_3/Bi_2MnSe_4 multilayer heterostructures, New J. Phys. **19**, 085002 (2017).

[10] T. Hirahara *et al.*, Large-gap magnetic topological heterostructure formed by subsurface incorporation of a ferromagnetic layer, Nano Lett. **17**, 3493 (2017).

[11] Y. Hou and R. Wu, Axion insulator state in a ferromagnet/topological insulator/antiferromagnet heterostructure, Nano Lett. **19**, 2472 (2019).

[12] C. D. Wagner, L. E. Davis, M. V. Zeller, J. A. Taylor, R. H. Raymond, and L. H. Gale, Empirical atomic sensitivity factors for quantitative analysis by electron spectroscopy for chemical analysis, Surf. Interface Anal. **3**, 211 (1981).

[13] I. Horcas, R. Fernandez, J. M. Gomez-Rodriguez, J. Colchero, J. Gomez-Herrero, and A. M. Baro, WSXM: A software for

scanning probe microscopy and a tool for nanotechnology, Rev. Sci. Instrum. **78**, 013705 (2007).

[14] Q. D. Gibson, L. M. Shoop, A. P. Weber, H. Ji, S. Nadj-Perge, I. K. Drozdov, H. Beindenkopf, J. T. Sadowski, A. Fedorov, A. Yazdani, T. Valla, and R. J. Cava, Termination-dependent topological surface states of the natural superlattice phase Bi_4Se_3, Phys. Rev. B **88**, 081108 (2013).

[15] L. A. Walsh, M. C. Smyth, T. A. Barton, Q. Wang, Z. Che, R. Yue, J. Kim, M. J. Kim, R. M. Wallace, and C. L. Hinke, Interface chemistry of contact metals and ferromagnets on the topological insulator Bi_2Se_3, J. Phys. Chem. C **121**, 23551 (2017).

[16] See Supplemental Material at http://link.aps.org/supplemental/10.1103/PhysRevMaterials.4.054001 for XPS survey spectra for all samples and detailed region scans near the C 1*s* region showing Se Auger electron features.

[17] R. Tarasenko, M. Vališka, M. Vondráček, K. Horáková, V. Tkáč, K. Carva, P. Baláž, V. Holý, G. Springholz, V. Sechovský, and J. Honolka, Magnetic and structural properties of Mn-doped Bi_2Se_3 topological insulators, Physica B **481**, 262 (2016).

[18] M. Taguchi, T. Uozumi, and A. Kotani, Theory of x-ray photoemission an x-ray emission spectra in Mn compounds, J. Phys. Soc. Jpn. **66**, 247 (1997).

[19] A. S. Hewitt, J. Wang, J. Boltersdorf, P. A. Maggard, and D. B. Dougherty, Coexisting Bi and Se surface terminations of cleaved Bi_2Se_3 single crystals, J. Vac. Sci. Technol. B **32**, 04E103 (2014).

[20] S. Babakiray, T. A. Johnson, P. Borisov, M. B. Holcomb, D. Lederman, M. A. Marcus, and K. Tarafder, Structural properties of $Bi_{2-x}Mn_xSe_3$ thin films grown via molecular beam epitaxy, J. Appl. Phys. **118**, 045302 (2015).

[21] K. Momma and F. Izumi, VESTA 3 for three-dimensional visualization of crystal, volumetric and morphology data, J. Appl. Crystallogr. **44**, 1272 (2011).

[22] D. J. O'Hara, T. Zhu, A. H. Ahmed, Y. K. Luo, C. H. Lee, M. R. Brenner, S. Rajan, J. A. Gupta, D. W. McComb, and R. K. Kawakami, Room temperature intrinsic ferromagnetism in epitaxial manganese selenide films in the monolayer limit, Nano Lett. **18**, 3125 (2018).

[23] O. Kubachewski, C. B. Alcock, and P. J. Spencer, *Materials Thermochemistry*, 6th ed. (Pergamon, Oxford, 1993).

[24] A. Olin, B. Noläng, E. G. Osadchii, L. O. Öhman, and E. Rosén, *Chemical Thermodynamics Volume 7: Chemical Thermodynamics of Selenium*, edited by F. J. Mompean, J. Perrone, and M. Illemassene (Elsevier, Amsterdam, 2005), p. 34.

[25] A. R. Mellnik, J. S. Lee, A. Rchardella, J. L. Grab, P. J. Mintun, M. H. Fisher, A. Vaezi, A. Manchon, E.-A. Kim, N. Samarth, and D. C. Ralph, Spin-transfer torque generated by a topological insulator, Nature (London) **511**, 449 (2014).

[26] P. Li, J. Kally, S. S.-L. Zhang, T. Pillsbury, J. Ding, G. Csaba, J. Ding, J. S. Jiang, Y. Liu, R. Sinclair, C. Bi, A. DeMann, G. Rimal, W. Zhang, S. B. Field, J. Tang, W. Wang, O. G. Heinonen, V. Novosad, A. Hoffman, N. Samarth, and M. Wu, Magnetization switching using topological surface states, Sci. Adv. **5**, eaaw3415 (2019).

[27] W. Jiang, G. Chen, K. Liu, J. Zang, S. G. E. te Velthuis, and A. Hoffman, Skyrmions in magnetic multilayers, Phys. Rep. **704**, 1 (2017).

[28] K. Yasuda, R. Wakatsuki, T. Morimoto, R. Yoshimi, A. Tsukazaki, K. S. Takahashi, M. Ezawa, M. Kawasaki, N. Nagaosa, and Y. Tokura, Geometric Hall effects in topological insulator heterostructures, Nat. Phys. **12**, 555 (2016).

[29] M. Lang, M. Montazeri, M. C. Onbasli, X. Kou, Y. Fan, P. Upadhyaya, K. Yao, F. Liu, Y. Jiang, W. Jiang, K. L. Wong, G. Yu, J. Tang, T. Nia, L. He, R. N. Schwartz, Y. Wang, C. A. Ross, and K. L. Wang, Proximity induced high-temperature magnetic order in topological insulator—Ferrimagnetic insulator heterostructure, Nano Lett. **14**, 3459 (2014).

[30] M. Mogi, T. Nakajima, V. Ukleev, A. Tsukazaki, R. Yoshimi, M. Kawamura, K. S. Takahashi, T. Hanashima, K. Kakurai, T. H. Arima, M. Kawasaki, and Y. Tokura, Large Anomalous Hall Effect in Topological Insulators with Proximitized Ferromagnetic Insulators, Phys. Rev. Lett. **123**, 016804 (2019).

[31] X. Yao, B. Gao, M. G. Han, D. Jain, J. Moon, J. W. Kim, Y. Zhu, S. W. Cheong, and S. Oh, Record high-proximity-induced anomalous Hall effect in $(Bi_xSb_{1-x})_2Te_3$ thin film grown on $CrGeTe_3$ substrate, Nano Lett. **19**, 4567 (2019).

[32] J. Li, Y. Li, S. Du, Z. Wang, B. L. Gu, Z. C. Zhang, K. He, W. Duan, and Y. Xu, Intrinsic magnetic topological insulators in van der Waals layered $MnBi_2Te_4$-family materials, Sci. Adv. **5**, eaaw5685 (2019).

[33] C. Liu, Y. Wang, H. Li, Y. Wu, Y. Li, J. Li, K. He, Y. Xu, J. Zhang, and Y. Wang, Robust axion insulator and Chern insulator phases in a two-dimensional antiferromagnetic topological insulator, Nat. Mater. **19**, 522 (2020).

[34] Y. Deng, Y. Yu, M. Z. Shi, Z. Guo, Z. Xu, J. Wang, X. H. Chen, and Y. Zhang, Quantum anomalous Hall effect in intrinsic magnetic topological insulator $MnBi_2Te_4$, Science **367**, 895 (2020).

[35] T. Zhu, A. J. Bishop, T. Zhou, M. Zhu, D. J. O'Hara, A. A. Baker, R. C. Walko, J. J. Repicky, J. A. Gupta, C. M. Jozwiak, E. Rotenberg, J. Hwang, I. Žutić, and R. K. Kawakami, Magnetic properties and electronic structure of magnetic topological insulator $MnBi_2Se_4$, arXiv:2003.07938.